Deregulated Overexpression of hCdt1 and hCdc6 Promotes Malignant Behavior

Michalis Liontos,[1] Marilena Koutsami,[1] Maria Sideridou,[1] Konstantinos Evangelou,[1] Dimitris Kletsas,[3] Brynn Levy,[5] Athanassios Kotsinas,[1] Odelia Nahum,[5] Vassilis Zoumpourlis,[4] Mirsini Kouloukoussa,[1] Zoi Lygerou,[6] Stavros Taraviras,[6] Christos Kittas,[1] Jirina Bartkova,[7] Athanasios G. Papavassiliou,[2] Jiri Bartek,[7] Thanos D. Halazonetis,[8] and Vassilis G. Gorgoulis[1]

[1]Molecular Carcinogenesis Group, Department of Histology and Embryology, School of Medicine and [2]Department of Biochemistry School of Medicine, University of Athens; [3]Laboratory of Cell Proliferation and Ageing, Institute of Biology, National Centre for Scientific Research "Demokritos"; [4]Unit of Biomedical Applications, Institute of Biological Research and Biotechnology, National Hellenic Research Foundation, Athens, Greece; [5]Clinical Cytogenetics Laboratory, University of Columbia Medical Center, New York, New York; [6]Departments of General Biology and Pharmacology, School of Medicine, University of Patras, Patras, Greece; [7]Institute of Cancer Biology and Centre for Genotoxic Stress Research, Danish Cancer Society, Copenhagen, Denmark; and [8]Department of Molecular Biology, University of Geneva, Geneva, Switzerland

Abstract

The accurate execution of DNA replication requires a strict control of the replication licensing factors hCdt1 and hCdc6. The role of these key replication molecules in carcinogenesis has not been clarified. To examine how early during cancer development deregulation of these factors occurs, we investigated their status in epithelial lesions covering progressive stages of hyperplasia, dysplasia, and full malignancy, mostly from the same patients. Abnormal accumulation of both proteins occurred early from the stage of dysplasia. A frequent cause of unregulated hCdc6 and hCdt1 expression was gene amplification, suggesting that these components can play a role per se in cancer development. Overexpression of hCdt1 and hCdc6 promoted rereplication and generated a DNA damage response, which activated the antitumor barriers of senescence and apoptosis. Generating an inducible hCdt1 cellular system, we observed that continuous stimulus by deregulated hCdt1 led to abrogation of the antitumor barriers and resulted in the selection of clones with more aggressive properties. In addition, stable expression of hCdc6 and hCdt1 in premalignant papilloma cells led to transformation of the cells that produced tumors upon injection into nude mice depicting the oncogenic potential of their deregulation. [Cancer Res 2007;67(22):10899–909]

Introduction

Genomic stability is of primary importance for survival and proper functioning of all cells. The most deleterious type of DNA damage leading to genomic instability is the double-strand break (DSB; ref. 1). When DSBs occur, the DNA damage response (DDR) pathway is activated to eliminate the genomic threat (1). The DSB-DDR cascade consists of sensor proteins such as the Mre11/Rad50/Nbs1 complex and 53BP1, adaptor proteins including BRCA1 and MDC1/NFBD1, the apical signaling kinases ataxia-telangiectasia mutated (ATM) and DNA-protein kinase, and the effector kinase Chk2 (1). The main biochemical end effect of the DSB-DDR cascade is p53 activation (1). The outcome of the response may be either repair of damage (1), arrest in the form of accelerated senescence (2), or in case of extensive damage, apoptosis (1). We recently showed that DDR is an early inducible barrier in carcinogenesis alarmed due to compromised DNA replication (2–4).

Disruption of normal replication mechanism, a condition termed replication stress, can create a cellular environment prone to genomic instability. Thus, accurate execution of DNA replication is of paramount importance in maintaining genomic integrity. The process of DNA replication relies on the control of cyclin-dependent kinases, which regulate the molecules comprising the replication complexes (5). Two key proteins of the replication complex, the DNA replication licensing factors (RLF) hCdt1 and hCdc6, when recruited during G_1-S transition on the origin recognition complexes, facilitate the loading of the minichromosome maintenance proteins 2 to 7 on the chromatin, thereby licensing the origins to fire once per cell cycle (6). Deregulation of hCdc6 and/or hCdt1 may lead to origin nonfiring or refiring, resulting in DNA underreplication or overreplication. The ability of deregulated RLF overexpression to cause rereplication, as reported by Vaziri et al. (7), providing seeds for genomic instability, has been recently challenged (8). Lately, we observed that overexpression of hCdc6, among other factors, can cause replication stress that evokes DDR-mediated senescence (2). High levels of RLFs have been observed in various types of cancer (9–14); however, the issue of how early during cancer development deregulation of the RLFs takes place remains unresolved.

To answer the latter question, we investigated the status of both RLFs in human epithelial lesions covering the whole histopathologic spectrum of carcinogenesis and subsequently explored the ability of hCdc6 and/or hCdt1 to promote rereplication and induce genomic instability and tumor aggressiveness.

Materials and Methods

Tissue samples. Frozen and formalin-fixed, paraffin-embedded material from 75 non–small cell lung carcinomas and adjacent normal lung tissue, and corresponding precancerous lesions were used (3, 9). Ninety-six cases of nonfamilial colon lesions and 15 head-and-neck cases comprising normal, hyperplastic, dysplastic, and carcinoma counterparts (15) were randomly selected from the tissue banks of the Department of Histology-Embryology, Athens, Greece, and four institutes from Denmark and Norway, after local ethical committee approvals. Samples are presented

Note: Supplementary data for this article are available at Cancer Research Online (http://cancerres.aacrjournals.org/).

M. Liontos, M. Koutsami, and M. Sideridou contributed equally to this work.

Requests for reprints: Vassilis G. Gorgoulis, Molecular Carcinogenesis Group, Department of Histology and Embryology, School of Medicine, University of Athens, Antaiou 53 Str., Lamprini, Ano Patissia, GR-11146 Athens, Greece. Phone: 30-210-6535894; Fax. 30-210-6535894; E-mail: histoclub@ath.forthnet.gr or vgorg@med.uoa.gr.

doi:10.1158/0008-5472.CAN-07-2837

in Supplementary Table S1. None of the patients had undergone any cancer therapy before surgical resection of the lesions.

Cell lines. BJ, MCF7, HeLa, U2OS, and P1 cell lines were used. Cells were maintained in DMEM (Biochrome), with 10% FCS (Biochrome), 2 mmol/L L-Glutamine (Biochrome), and 100 μg/mL penicillin and streptomycin (Biochrome), respectively, at 37°C and 5% CO_2.

Plasmid construction. pBabeHyg-hCdc6 was constructed by digesting pCS3-hCdc6 (16) with *Bam*HI and *Xho*I and subcloning *hCdc6*-cDNA into pBabeHyg. *hCdt1*-cDNA was isolated from pCDEBΔ-hCdt1 (17) with *Xba*I and *Hin*dIII digestions and subcloned into pCB6. The later was digested with *Eco*RI to isolate the *hCdt1*-cDNA with ends compatible for subcloning into pBIB and pIRES2neo vectors, respectively. Finally, the pTRE2hyg-hCdt1 construct was obtained after excision of the *hCdt1*-cDNA from pIRES2neo, using *Cla*I and *Not*I digestions, and religation into pTRE2hyg.

Retrovirus construction and infections. BJ and U2OS cells were transiently transduced with *hCdc6* or *hCdt1* and the corresponding control vectors using the Phoenix helper-free retrovirus producer cell line, as previously described (2).

U2OS-TetON-hCdt1 inducible system. U2OS-TetON cells (Clontech) were transfected with pTRE2hyg-hCdt1 at ~80% confluence, using LipofectAMINE 2000 (Invitrogen). Hygromycin selection (200 mg/mL) was initiated 4 days later and clones emerged after 2 weeks. Expression of hCdt1 in stably transfected clones was confirmed with immunoblot and reverse transcription-PCR (RT-PCR) analysis.

Growth curve analysis. U2OS-TetON-hCdt1 cells, in the absence or presence of doxycycline, were seeded at day 0 on 60-mm Petri dishes at a density of 3×10^5. Every 3 days up to day 30, cells were trypsinized and counted, and 3×10^5 cells were reseeded. The ratio of cells counted versus the cells seeded was estimated at every subculture, and the total cell number was calculated by multiplying these ratios with the number of cells seeded initially.

Small interfering RNA transfection. U2OS-TetON-hCdt1 small interfering RNA (siRNA) transfection was done as per previous publication (2).

Immunohistochemistry and indirect immunofluorescence analysis. Immunohistochemistry and immunofluorescence analysis have been previously described (2, 4, 9, 18).

Antibodies. Primary antibodies for immunohistochemistry, immunofluorescence, and immunoblot analysis have been previously described (2, 3, 9, 13, 18, 19).

5-Bromo-2-deoxyuridine staining. Staining with 5-bromo-2-deoxyuridine (BrdUrd) was done as previously described (2).

Terminal deoxyribonucleotide transferase–mediated nick-end labeling assay. Double-stranded DNA breaks were detected by terminal deoxyribonucleotide transferase–mediated nick-end labeling (TUNEL), according to protocols described elsewhere (9).

Chromogenic and fluorescent *in situ* hybridization. Chromogenic *in situ* hybridization (CISH) analysis was done with the Zymed SPoT-Light HER2 CISH kit (Invitrogen) on formalin-fixed, paraffin-embedded tissue sections, following the manufacturer's instructions. Control reactions and evaluation were done according to the manufacturer's guidelines.

Senescence-associated β-galactosidase staining. Senescence-associated β-galactosidase (SA-β-gal) staining and evaluation was done as previously described (2).

Flow cytometry (fluorescence-activated cell sorting). Cells were harvested with trypsinization and centrifuged at 1,000 rpm for 5 min at room temperature. The pellet was resuspended in 500 μL PBS, fixed with 80% ethanol, vortexed, and stained with propidium iodide (50 μg/mL), in the presence of 5 mmol/L $MgCl_2$ and 10 μg/mL RNase A in 10 mmol/L Tris-HCl (pH 7.5). DNA content was analyzed on a FACSCalibur (Becton Dickinson) using the Modfit software.

Ploidy analysis. Ploidy analysis was done as previously described (18).

Protein extraction and immunoblotting. Total protein and histone extraction from frozen tissue samples was done according to protocols described elsewhere (3).

Nucleic acid extraction and cDNA preparation. Tissue microdissection and DNA extraction were done according to protocols described elsewhere (20). RNA and cDNA preparation have been previously described (20).

Differential PCR. *hCdc6/hCdt1* gene amplification was assessed by the differential PCR method, as previously used (20). Neoplastic samples scoring ≥2-fold difference from the corresponding normal counterpart were characterized as *hCdt1* and/or *hCdc6* gene-amplified cases and were also confirmed by real-time PCR (MJ-Research DNA-Engine-Opticon). Primers and annealing temperatures are given in Supplementary Table S2.

Comparative RT-PCR and real-time RT-PCR. Evaluation of *hCdt1* and *hCdc6* mRNA status was done by a semiquantitative RT-PCR method previously described (20). Two reference genes, *GAPDH* and *PBGD*, were used to validate the results. Neoplastic samples scoring ≥2-fold *hCdt1* and/or *hCdc6* increased expression from the corresponding normal counterpart were characterized as overexpressed and where verified by real-time PCR (MJ-Research DNA-Engine-Opticon; data not shown). Primers and annealing temperatures are given in Supplementary Table S2.

Pulsed-field gel electrophoresis. U2OS cells (1×10^6) were inserted into 1% w/v low-melting-agarose plugs (Sigma) and incubated in 0.5 mol/L EDTA, 1% *N*-laurylsarcosyl and 1 mg/mL proteinase K at 50°C for 48 h. Plugs were washed four times in TE (10 mmol/L and 1 mmol/L) buffer and the DNA was separated in 1% agarose (Invitrogen), 0.5 × Tris-borate EDTA (TBE: 45 mmol/L Tris-borate, 1 mmol/L EDTA) by pulsed-field gel electrophoresis, using a CHEF DRIII apparatus and a Mini Chiller model 1000 with a variable speed pump (Bio-Rad). Electrophoresis was conducted in 0.5× TBE at 14°C, 4 V/cm, with a fixed angle of 120°, with a switching time 240 s for 18 h. Gels were stained for 30 min with ethidium bromide and assessed under UV light.

Comparative genomic hybridization. Comparative genomic hybridization (CGH) was done as previously described (3).

Single nucleotide polymorphism oligonucleotide microarray analysis. U2OS cell line is highly aneuploid and hypertriploid (21). DNA was extracted from induced and noninduced cultures at 0, 17, and 30 days. All samples were assayed using the Mapping 250K Sty Assay Kit.[9] The assay was done according to the manufacturer's protocol. Detection of copy number changes was done with Chromosome Copy Number Analysis Tool version 4.0, [9] using pairwise comparisons of test (17 days induced/noninduced and 30 days induced/noninduced) and reference data (0 days) and default settings. Output data comprised smoothed log 2 ratio values, median log 2 ratio values of all contiguous single nucleotide polymorphisms (SNP) in the given HMM copy number state segment, and the HMM copy number state.

Invasion assay. The cellular invasion potential was estimated with a cell invasion assay kit (Chemicon), following the manufacturer's instructions.

Tumorigenicity assay. P1-hCdt1, P1-hCdc6, and corresponding mock counterparts were harvested, washed in PBS, and s.c. injected (1×10^6 cells) at two sites in the abdominal region of male severe combined immunodeficient (SCID) mice. Tumor growth was measured twice to thrice weekly. Tumorigenicity for each cell type was tested in five animals, respectively.

Statistical analysis. Statistical analysis was done with SPSS 12.0 software.

Results and Discussion

Deregulated overexpression of the RLFs, hCdt1 and hCdc6, is an early event in carcinogenesis. Recently, we showed that hCdt1 and hCdc6 are overexpressed in a significant proportion of lung carcinomas (9). To determine at what stage during carcinogenesis deregulation of the RLFs hCdc6 and hCdt1 occurs, we did an immunohistochemical analysis in precancerous lesions (hyperplasias and dysplasias) located adjacent to the lung carcinomas (3; Supplementary Table S1). Their location suggested that they were precursors of the malignancy developed in the

[9] http://www.affymetrix.com

patients. Similar analysis was done in precancerous and cancerous lesions from the larynx and colon (Supplementary Table S1). The laryngeal premalignant and malignant specimens were from the same patient, whereas the colon lesions were not.

A clear nuclear hCdct1 and/or hCdc6 signal was evident from the stage of dysplasia in all three types of cancer studied (Fig. 1; Supplementary Table S1). In cases stained positive for RLFs, immunoexpression extended always from the dysplastic area to the adjacent cancerous region and was never restricted to the cancerous area. No signal was observed in the normal epithelium or adjacent hyperplastic lesions of the lung and larynx. In normal colon, hCdt1 was present in the nuclei of a limited number of cells, located in the proliferative compartment of the crypt, as previously shown (14), whereas hCdc6 was not detectable. In lung and laryngeal lesions, the percentage of positive cells increased from dysplasias to carcinomas (Fig. 1*A* and *B*). In colon, expression was elevated from grade 1 adenomas to grade 3, whereas in the carcinomas their immunohistochemical status was slightly reduced (Fig. 1*C*). Interestingly, a subcellular shift was observed in the staining of hCdc6 from the nuclei, mainly in dysplasias, to the cytoplasm in carcinomas (Fig. 1*A* and *C*). Physiologically, hCdc6, after taking part in the replication licensing process, has been suggested to translocate to the cytoplasm for degradation (22). The cytoplasmic expression of hCdc6 has been previously observed in lung (9, 10) and cervical carcinomas (11) and probably represents aberrant accumulation of the protein (9) due to S-phase deregulation.

The absence of signal in the hyperplasias and normal tissues could mean that the levels of both factors were below the threshold of immunohistochemical identification. In our previous study, we showed that hCdc6 immunopositivity was restricted to cases that exhibited markedly increased levels (>4-fold) of the protein, as assessed by immunoblotting (9). To explore whether the absence of staining was due to levels below the immunohistochemical threshold, we examined the expression of *hCdt1* and/or *hCdc6*, by RT-PCR, in five cases with positive immunohistochemistry signal for both factors in the dysplastic and cancerous areas (Supplementary Fig. S1*A*). The cases comprised lesions covering the whole histopathologic spectrum of alterations. The RT-PCR method was chosen because immunoblotting requires significant amount of tissue, which is difficult to retrieve from such small lesions. The results showed an increase of ~2-fold for both hCdc6 and hCdt1 mRNA levels in the hyperplasias compared with the adjacent normal tissue (Supplementary Fig. S1*A*), which justifies, according to our previous observation (9), the absence of immunohistochemical signal. On the other hand, the hCdt1 and hCdc6 levels in the adjacent dysplastic and cancerous area increased abruptly (>5-fold; Supplementary Fig. S1*A*).

Given the hCdt1 and hCdc6 role in replication, one could argue that increased immunodetection from dysplasia to cancer could merely reflect an increase in proliferation rate. However, no correlation was found with the proliferation marker Ki-67 (data not shown), confirming previous observations in carcinomas (9, 10, 12). Moreover, the preferential staining in certain lesions (dysplasias and cancer) and not in normally proliferating tissues or even hyperplasias suggests that immunohistochemical detection depicts abnormal overexpression of the proteins.

Thus, our results suggest that in very early precursor lesions (hyperplasias), the moderate increase of hCdt1 and hCdc6 (Supplementary Fig. S1*A*) possibly reflects a deranged/accelerated cell turnover, owed to local mitotic overload, leading to a potentially reversible disruption of tissue homeostasis (3), whereas in advanced lesions (dysplasia and cancer) their significant overabundance (Fig. 1; Supplementary Fig. S1) probably results either from deregulation of transcription factors controlling their expression or from abrupt genomic changes, such as gene amplification.

Gene amplification is a frequent cause of deregulated hCdt1 and hCdc6 overexpression. The pivotal transcriptional activators of *hCdt1* and *hCdc6* are the E2F members E2F-1 and E2F-2 (23). Overexpression of E2F-1 and E2F-2 has been observed in various epithelial malignancies (23). Therefore, hCdt1 and hCdc6 transcriptional deregulation, due to deranged E2F expression, could be a source of their abnormal overproduction (24). Nonetheless, there are no reports examining whether gene amplification could constitute an alternative mechanism of deregulated overexpression. To this end, we did a differential PCR assay in our lung cancer data base, previously analyzed for hCdt1 and hCdc6 expression (9). We found a 2.5- to 4.5-fold gene amplification of *hCdc6* in 18 of 38 hCdc6-overexpressing cases (47%), whereas no amplification was observed in the specimens showing normal hCdc6 levels (Fig. 2*A* and *B*). Similarly, a 2.5- to 4-fold amplification of *hCdt1* was seen in 9 of 32 samples overexpressing hCdt1 (28%), whereas there was no *hCdt1* amplification in the hCdt1 normally expressing cases (Fig. 2*A* and *B*). Both findings were confirmed by real-time PCR (Supplementary Fig. S1*B*). Concomitant amplification of both genes was noticed in six cases (19%).

Given that *hCdc6* is located in the proximity of *c-erbB2* on *17q21.3*, which is frequently amplified in human cancer, we set to examine whether *hCdc6* gene amplification is a secondary event to *c-erb2* gene amplification. Therefore, we did a *c-erb2* CISH in the cases, which showed *hCdc6* gene amplification with differential PCR. Interestingly, CISH showed polysomy of chromosome 17 in 57% of these cases, whereas in the remaining samples *c-erb2* gene amplification was not noticed (Fig. 2*C*). The last result was also confirmed by differential PCR, as well (Fig. 2*C*). Notably, polysomy of chromosome 17 is observed in HeLa cells, which display high expression levels of hCdc6 (Fig. 2*C*).

To analyze in detail the genomic profile of tumors with gene amplification, we did a high-resolution CGH analysis in the six specimens that exhibited gene amplification for both genes. CGH showed amplification of the broader chromosomal region encoding *hCdc6* in two of the examined specimens (Fig. 2*D*), suggesting that besides *hCdc6* and *c-erb2* other putative oncogenes may lay in this area. On the other, CGH revealed some intriguing findings regarding *hCdt1*. The *16q13-24.1/2* region was found deleted in three samples, whereas *16q24.3*, which lies in the vicinity of this area and contains *hCdt1*, was always spared (Fig. 2*D*). The *16q* chromosomal arm is frequently lost in many tumor types as it contains a tumor-suppressor gene cluster proximal to the fragile site *FRA16D* (25). These findings indicate that hCdt1is likely essential for cancer cells. The lack of correlation between CGH and differential PCR with respect to *hCdt1* is possibly due to the limitation of the particular method to detect genomic changes affecting less than a few megabases (26).

Altogether, the above findings suggest that *hCdc6* amplification can be a primary discrete event during carcinogenesis, and that gene amplification represents a frequent cause of hCdc6 and hCdt1 unregulated overexpression, at least in one tumor type.

Deregulated hCdt1 and hCdc6 overexpression generates DSBs activating the DDR checkpoint. Gene amplification is a hallmark of tumor cells and genes undergoing amplification are

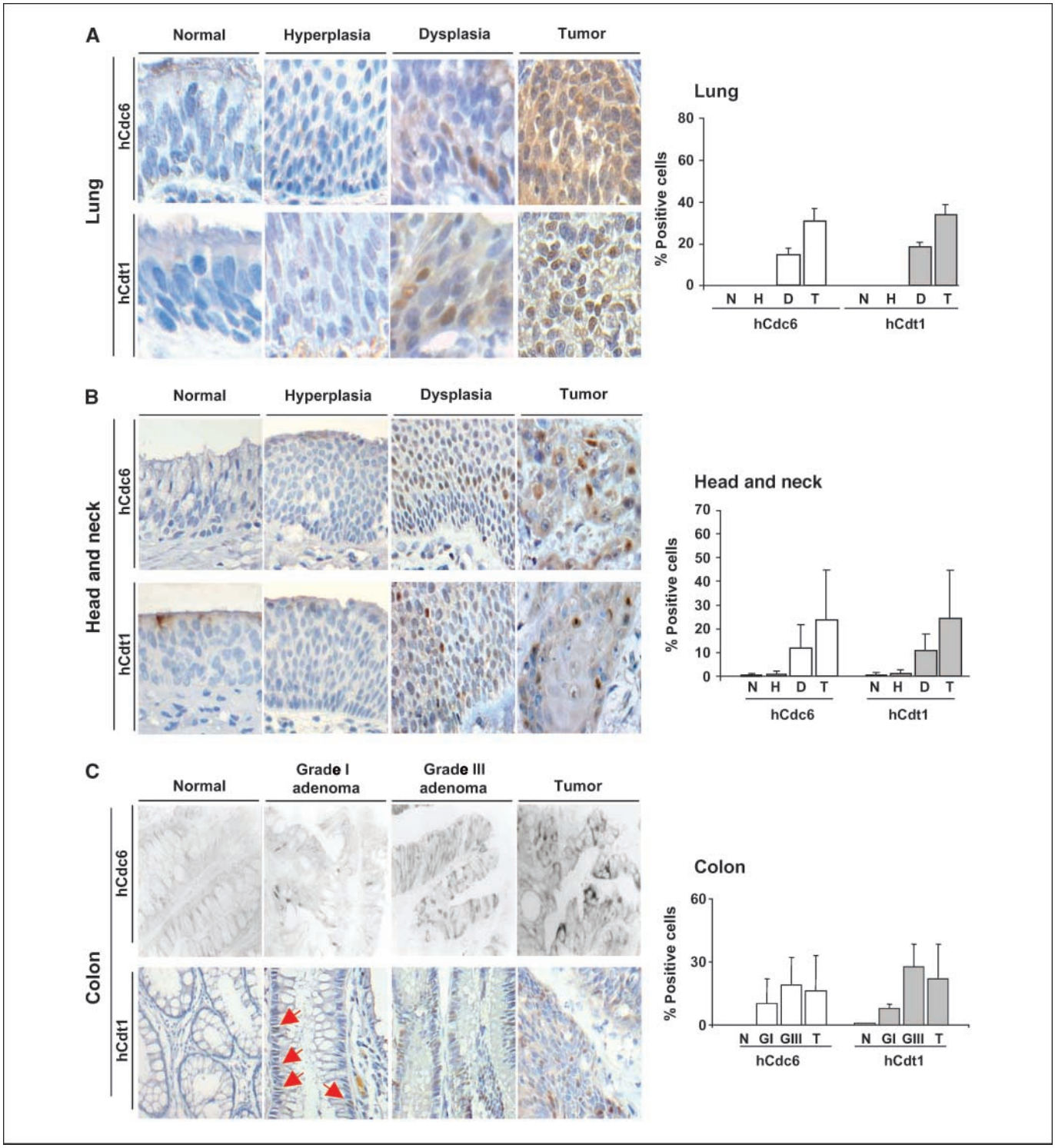

Figure 1. hCdt1 and hCdc6 overexpression is an early event during carcinogenesis. Immunohistochemical analysis of hCdc6 and hCdt1 in normal, hyperplastic, dysplastic, and cancerous lesions of the lung (*A*), larynx (*B*), and colon (*C*). *Columns,* mean of the percentages of cells staining positive for hCdc6 and hCdt1 in the aforementioned lesions; *bars,* SD. *Red arrows,* in grade 1 colonic adenoma, immunopositivity for hCdt1. *N,* normal tissue; *H,* hyperplastic tissue; *D,* dysplastic tissue; *GI,* grade 1 and 2 adenoma (mild to moderate dysplasia, representing low grade dysplasia, *LGD*); *GIII,* grade 3 adenoma (severe dysplasia, representing high grade dysplasia, *HGD*); *T,* tumor tissue.

considered as candidate oncogenes. Whether hCdt1 or hCdc6 overexpression can act in an oncogenic manner endowing the cells with capacity to promote carcinogenesis is unclear. Studies examining the transformation potency of *hCdt1* are controversial (24). We recently showed that expression of hCdc6 in diploid fibroblasts activates the DNA damage checkpoint inducing a senescence phenotype (2), supporting its oncogenic role. Here, we show a similar phenomenon for hCdt1, after introducing it in BJ

normal diploid fibroblasts by retroviral infection (Supplementary Fig. S2*A*).

However, experiments in primary cells cannot clearly define the role of hCdt1 and hCdc6 overexpression in tumorigenesis because, as presented earlier, the shift from regulated to deregulated RLF overexpression occurs later between the stage of dysplasia and the onset of cancer. Defining the time point of a particular molecular alteration is of great importance in understanding its role in the natural history of each tumor type. It has been suggested that aberrant overexpression of RLFs could favor cancer progression by promoting genetic instability via rereplication (7). Nevertheless, the ability of hCdt1 to induce rereplication and generate DSBs was questioned recently (8). To clarify this issue and examine the potential of the RLFs to induce genomic instability, we introduced *hCdt1* and *hCdc6* into the U2OS human osteosarcoma cell line. We favored these cells because their genetic background (*p53* intact, pRb hyperphosphorylated, and $p16^{INK4A}$ lost; ref. 19) resembles the genetic profile of high-grade dysplastic-early cancer lesions seen in many types of cancer such as those of the respiratory track (27, 28). Thus, the events following introduction of *hCdt1/hCdc6* would simulate closer the *in vivo* observations. In addition, the U2OS is a low endogenous DDR activity cellular system (29), thus facilitating its evaluation after introducing putative oncogenes.

hCdt1 and hCdc6 were expressed, separately, in the U2OS cells by recombinant retrovirus infection. After successful infection confirmation (Supplementary Fig. S2*B*), cells were collected for flow cytometry to examine rereplication. Analysis revealed an increase in the S-phase fraction and in the cells with a DNA content >4n (Supplementary Fig. S2*C*). These findings suggest an S-phase arrest with partially replicated DNA and some degree of rereplication without mitosis. Inability to enter mitosis was confirmed with induction of the Tyr^{15}-phosphorylated, inactive form of the key mitosis-promoting kinase cdc2 (ref. 30; Supplementary Fig. S2*C*). The degree of rereplication was not as high as previously reported, probably because p53, which is wild-type in U2OS, protects the cells from extensive rereplication (7). To test whether these events led to DNA damage checkpoint activation, we measured the levels of γH2AX, Chk2-pT68, and pS15-p53. Indeed, their protein expression levels were higher compared with the mock-infected cells (Supplementary Fig. S2*B*). Similar results were observed in MCF-7 human breast cancer cells transfected with hCdt1 and hCdc6 expressing vectors, separately or together (Supplementary Fig. S3). Because ATM is activated not only by DSBs but also by topological changes in chromatin structure (31), the checkpoint components could well be activated in such an alternative manner. To test the latter, pulsed-field gel electrophoresis was done in the infected cells. Damaged DNA was evident in both cases (Supplementary Fig. S2*B*), suggesting that rereplication leads to replication fork collapse and DSB formation, which eventually activate the DNA damage checkpoint.

Prolonged hCdt1 overexpression leads to a more aggressive phenotype, bypassing the antitumor barriers of accelerated senescence and apoptosis. The link between DDR activation and

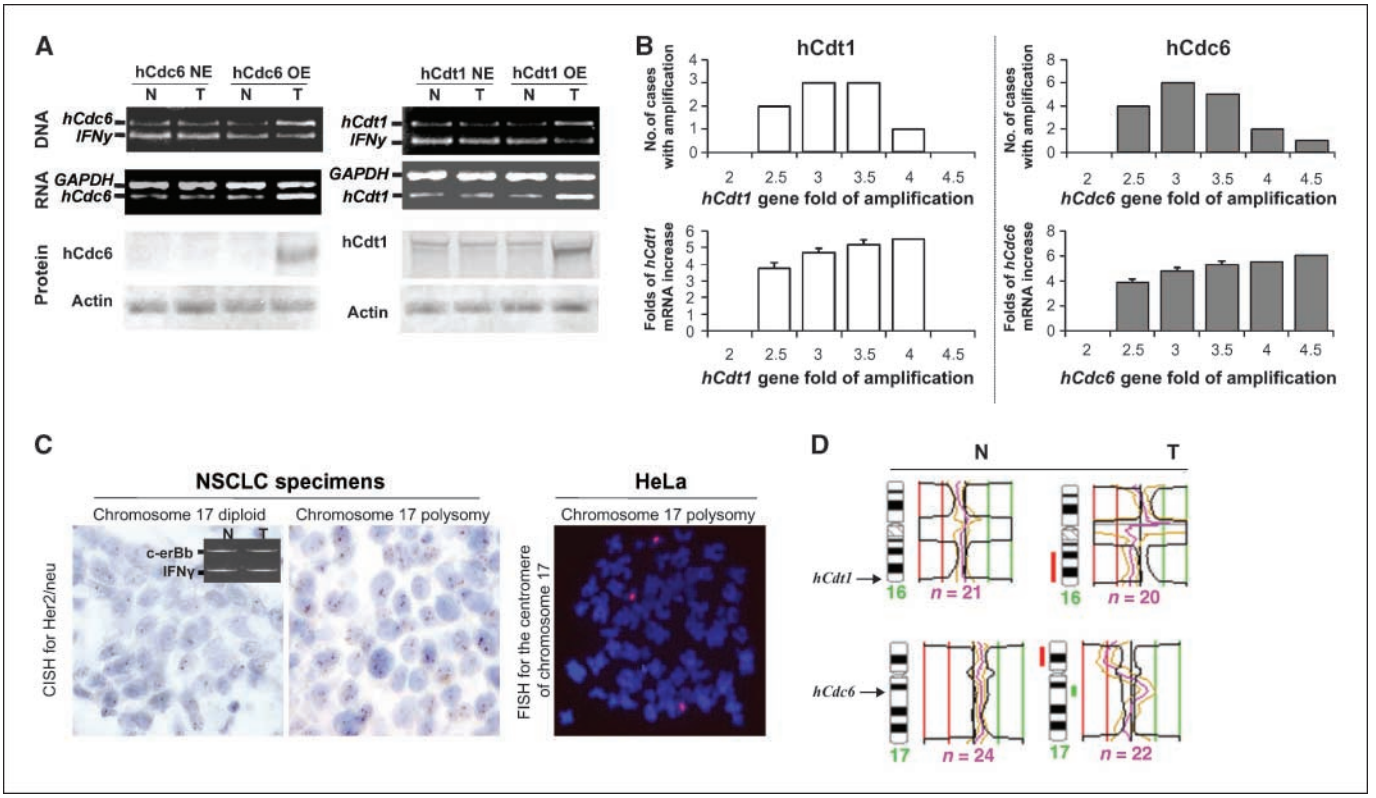

Figure 2. *hCdt1* and *hCdc6* are frequently amplified in lung cancer. *A,* differential PCR, RT-PCR, and immunoblotting indicating *hCdt1* and *hCdc6* amplification and overexpression. *NE,* normal expression; *OE,* overexpression; *N,* normal tissue; *T,* tumor tissue. *B,* the fold of *hCdc6* and *hCdt1* gene amplification and mRNA increase observed in the corresponding cases. *C,* chromosome 17 CISH analysis with a *c-erb2* probe in cases with *hCdc6* gene amplification and in the HeLa cell line. Differential PCR in embedded picture shows absence of c-erb2 amplification. *D,* CGH analysis in representative cases of lung cancer and their corresponding normal tissue. Only the chromosomes of interest are presented. *Red line,* chromosomal loss; *green line,* chromosomal gain; *n,* number of cells analyzed.

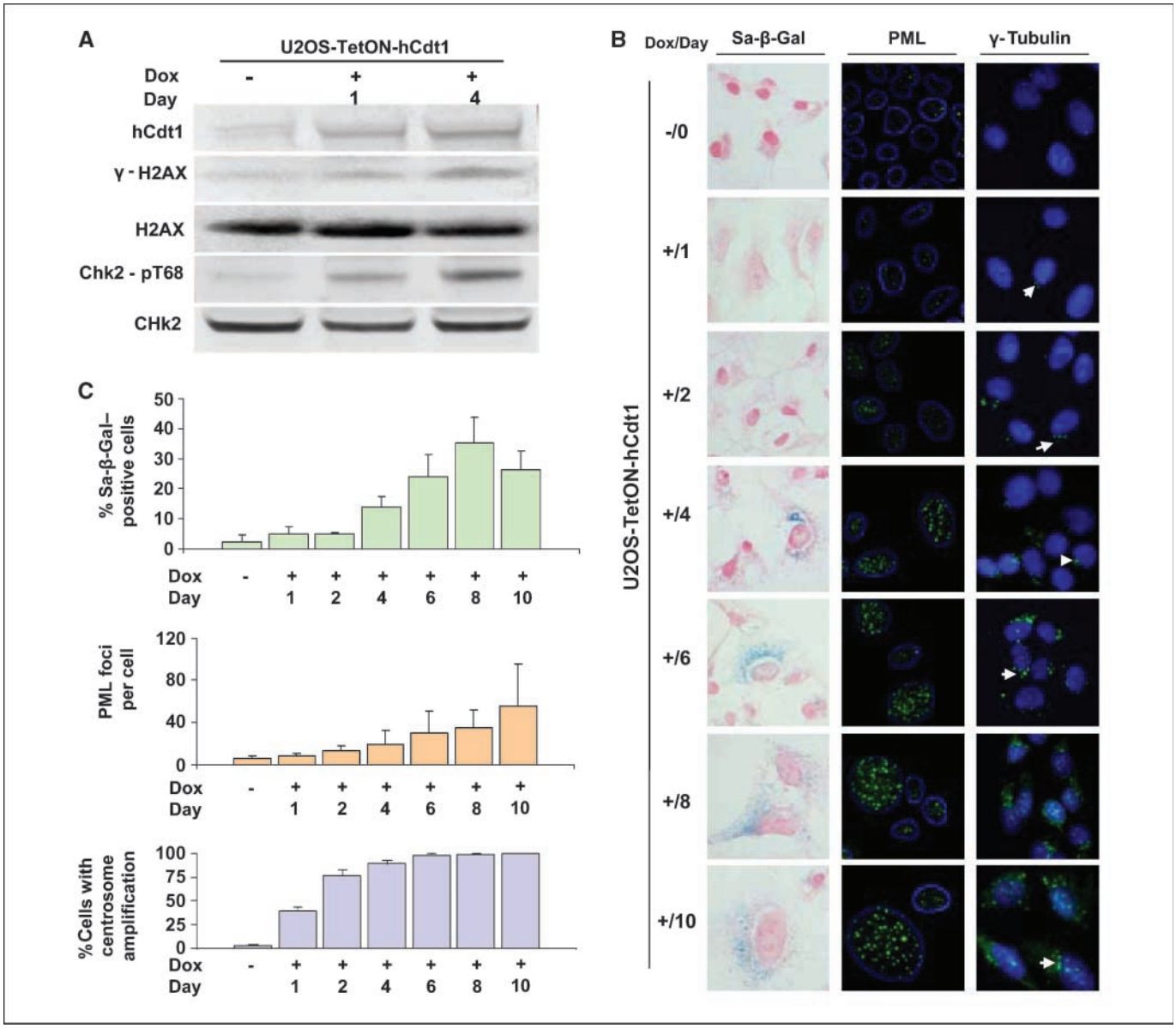

Figure 3. U2OS-TetON-hCdt1 cells with and without doxycycline (*Dox*) treatment, monitored in the first 10 d of the experiment. *A,* immunoblot analysis for hCdt1, γ-H2AX, and Chk2-pT68 expression (*H2AX* and *Chk2,* loading controls). *B,* SA-β-gal staining and immunofluorescence staining for PML and γ-tubulin (*arrows,* aggregates of centrosomes). *C, columns,* mean of cells with positive SA-β-gal staining, foci of PML bodies per cell, and centrosome amplification, respectively; *bars,* SD.

tumorigenesis (2–4, 32) implies that continuous DNA damage checkpoint activation could lead to selective suppression of the DDR-induced antitumor barriers, by inactivating mutations, resulting in genomic instability and tumor progression.

To examine whether prolonged expression of RLFs could create such a sequence of events, we developed an inducible hCdt1-U2OS cellular system in which hCdt1 was expressed by addition of doxycycline. We chose hCdt1 to generate the Tet-ON system, because ectopic expression of hCdt1 is more potent in inducing rereplication than that of hCdc6 (7) and because the expression of endogenous hCdt1 is tightly regulated *in vivo* (24). The expression levels of hCdt1 increased 4- to 5-fold, upon doxycycline induction (Supplementary Fig. S4), a ratio similar to that found in dysplastic and cancerous samples when compared with normal tissue or hyperplasia (Supplementary Fig. S1*A*; ref. 9). The degree of overexpression achieved mimics closer the clinical scenarios than the 20- to 100-fold increase reported previously (7, 8), which is most unlikely to occur *in vivo*.

The hCdt1 effects were monitored for 30 days. Within 24 h after hCdt1 induction, the DNA damage checkpoint became activated, as assessed by γ-H2AX and Chk2-pT68 levels (Fig. 3*A*). Activation of the checkpoint was more prominent over the following days (Fig. 3*A*). Two days after hCdt1 induction, the cells underwent morphologic changes with flattening and enlargement of the cytoplasm. By day 4, they adapted a clear senescence phenotype, as shown by SA-β-gal activity (Fig. 3*B*). The percentage of senescent cells increased over the days culminating at day 8 (Fig. 3*C*). Additionally, promyelocytic leukemia (PML) bodies, whose number and size increases in ras-senescent cells (33, 34), increased by number and size in hCdt1-overexpressing cells, also (Fig. 3*B*

and *C*). The increase of PML nuclear bodies also indicates that DNA damage occurs because they are associated with DNA lesions and repair (35, 36). Between days 8 and 15, an escalation in apoptosis was denoted, as assessed by fluorescence-activated cell sorting (FACS) and TUNEL assays, and accompanied by a small decrease in the senescent-cell population (Supplementary Fig. S4*B*). ATM-siRNA transfection of the induced cells resulted in almost complete abrogation of senescence and apoptosis (Supplementary Fig. S4*C*). Given that the U2OS cells are null for the senescence-linked proteins $p16^{INK4A}$ and $p14^{ARF}$ (37, 38), our results extend, using a novel candidate oncogene, and corroborate our concept of oncogene-induced DDR as an anticancer barrier (2–4).

After induction, FACS analysis showed an increase in the S-phase fraction and in number of cells with DNA content >4n (Supplementary Fig. S4*B*). According to a model, delay in S-phase progression, accompanied by pRb pathway defects, could lead to centrosome amplification (39). Because U2OS cells have the pRb pathway defective, due to $p16^{INK4A}$ loss (20), and a normal centrosome profile by default (18), we examined the above hypothesis by staining the cells with γ-tubulin to identify the number of centrosomes. Untreated U2OS-hCdt1 cells carried one or two centrosomes per cell, as previously reported (18). After 24 h of hCdt1 induction, 40% of the cells presented centrosome abnormalities. At day 4, ~90% of the cells harbored an abnormal centrosomal profile (structural and/or numerical aberrations, excess pericentriolar material), which by days 8 and 10 was present in almost all cells (Fig. 3*B* and *C*). Given the dominant role of centrosomes in chromosome segregation (39), these results suggest that deregulated hCdt1 expression, in addition to recombination-prone rereplicated DNA, could create an environment permissive for chromosomal instability also due to centrosome amplification.

Between days 10 and 15, the population of senescent and apoptotic cells, as assessed by SA-β-gal, FACS, and TUNEL assays, gradually decreased, and around days 25 to 30 exhibited the lowest values (Supplementary Fig. S5). Monitoring the growth properties of the hCdt1-induced cells, we observed, between days 6 to 15, a growth and BrdUrd incorporation retardation, which coincide with the senescence and apoptosis events described above (Supplementary Fig. S5*A* and *B*). Beyond this latter time point, BrdUrd incorporation increased and cells started to grow at a higher rate than the hCdt1 noninduced cells (Supplementary Fig. S5*A* and *B*). Moreover, such emerging "adapted" cells showed nuclear atypia characterized by micronuclei, lobulated nuclei, and nucleoplasmic bridges (Fig. 4*A* and *B*). The noninduced cells did not show

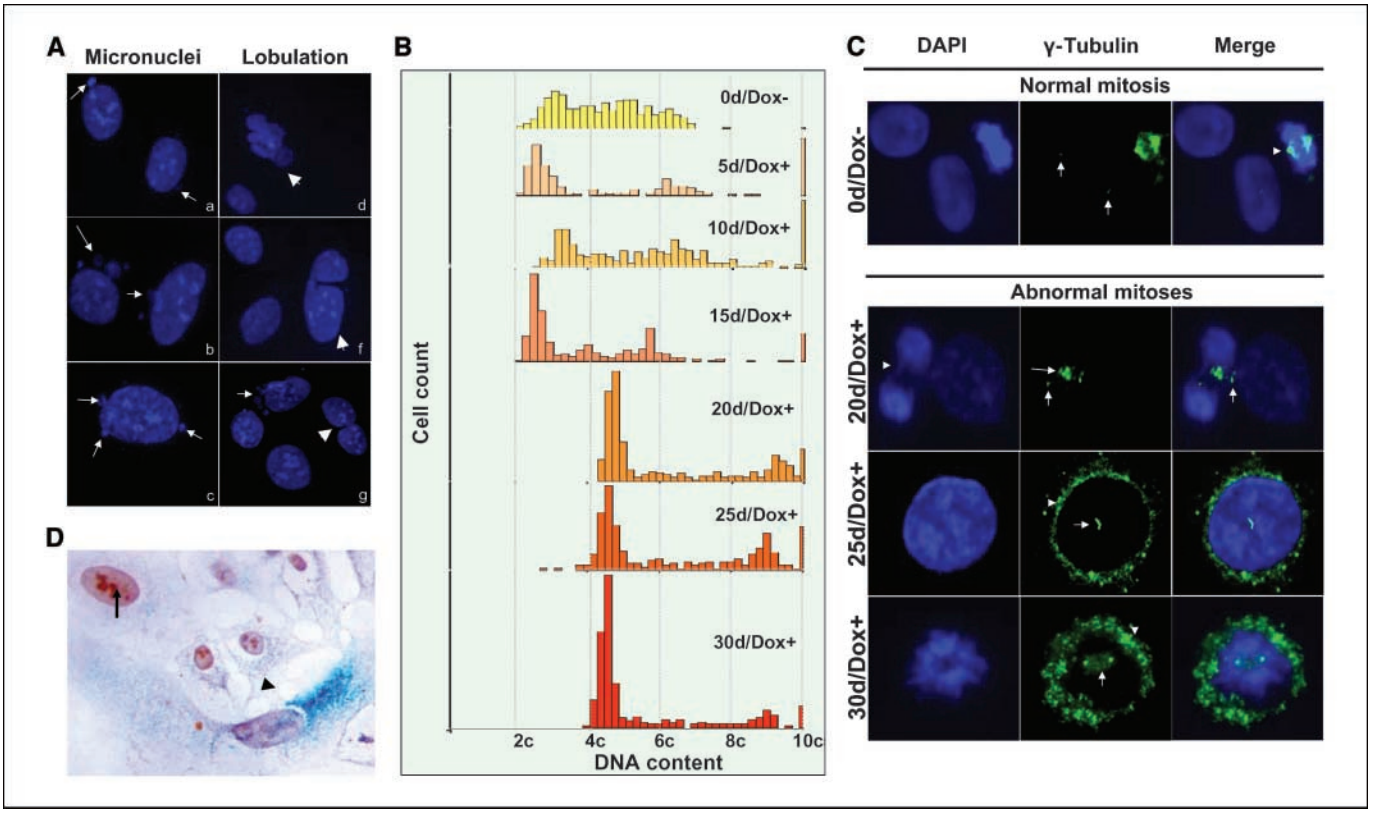

Figure 4. Prolonged overexpression of hCdt1 induces genomic instability. *A,* micronuclei (*arrows* in *A–C*) and lobulated nuclei (*arrowheads* in *D–G*) in U2OS-TetON-hCdt1 cells after 15 d of continuous hCdt1 induction. *B,* DNA content analysis, as assessed by Feulgen staining, in the induced U2OS-TetON-hCdt1 cellular system showing a gradual shift to polyploidy (>4C). *C,* images with representative morphologic characteristics, in noninduced and after prolonged (>15 d) hCdt1 induction, of U2OS-TetON-hCdt1 cells, after γ-tubulin immunofluorescence and 4′,6-diamidino-2-phenylindole (*DAPI*) staining (magnification, ×610). Day 0, control U2OS-TetON-hCdt1 cells, free of doxycycline, harbor one or two centrosomes per cell (*arrows*) and normal bipolar mitoses (*arrowhead*). Day 20 (*20d*), nucleoplasmic bridges (*arrowhead*). The two anaphasic nuclei are abnormally segregated because (see the corresponding γ-tubulin and merged photos) three centrosomes are visible next to the one anaphasic nucleus, whereas the other harbors only one centrosome. Next to them, a cell with two centrosomes (*merged, arrow*). Day 25 (*25d*), a large cell with four prominent centrosomes (*arrow*) and centriolar material forming a "beaded necklace" around the nucleus (*arrowhead*). Day 30 (*30d*), aberrant tetrapolar mitosis characterized by centrosome aggregates (*arrowhead*) in a ring formation. Semicondensed chromatin does not manage to locate in the middle of the central spindle (*arrow*). *D,* mutual exclusive staining of Ki-67 (*arrow*) and SA-β-gal (*arrowhead*) in U2OS-TetON-hCdt1 doxycycline-positive cells. Cells of smaller size Ki-67–positive are also observed (magnification, ×400).

such alterations, excluding the possibility that these features were due to cell culture propagation. Additionally, compared with control noninduced cells, which displayed normal bipolar mitoses (Fig. 4*C*), 10% to 13% of the induced cells exhibited after day 20 aberrant mitoses, characterized mainly by multipolarity (Fig. 4*C*). These nuclear features are indicative of chromosomal instability and are consistent with the ability of these cells to bypass the DNA damage checkpoint (40, 41). Simultaneously, in comparison with the noninduced cells, the DNA content histograms of the hCdt1-induced cells, as assessed by Feulgen staining, exhibited a rightward shift, from hypo/triploid values (2c–6c), at day 0 (21), to values larger than 4c, after day 20 (Fig. 4*B*). A significant proportion of cells contained DNA between 4c and 6c, with four and six prominent centrosomes (Fig. 4*B* and *C*), respectively. These results are indicative of S- and M-phase uncoupling leading to polyploidy, due to endoreduplication (42). Depending on the cell cycle checkpoint(s) status and the apoptotic machinery integrity, these cells will either die by mitotic catastrophe or survive, dividing asymmetrically and giving rise to aneuploid offsprings (42). The polyploid population, in our experimental setting, emerged mainly when the antitumor barriers of apoptosis and senescence were suppressed (Fig. 4*B*), contained increased number of centrosomes, and stained positive for Ki-67 (Fig. 4*D*), strongly suggesting that such cells follow the aneuploidy route. Supporting the above, the levels of p53, the downstream effector of the DDR pathway, showed a stepwise reduction after day 10, despite expression of hCdt1 and γ-H2AX (Fig. 5*A*; Supplementary Fig. S6).

According to a report, genotoxic insult–generated polyploidy probably represents an important recombination repair response (43). hCdt1-induced genomic recombination could take place between homologous regions favored by the presence of rereplicated DNA (7). Because rereplicated DNA produces DNA damage (Supplementary Fig. S2*B*), we presumed that cells possessing rereplicated DNA above a critical threshold should be "neutralized" by either senescence or apoptosis, whereas cells with rereplicated elements below a critical threshold would be prone to recombination processes leading to genomic instability. These events would favor the selection of cells resistant to hCdt1-induced apoptosis or senescence. To examine the hypothesis that genomic instability is induced by deregulated hCdt1, we did a SNP oligonucleotide microarray analysis of the DNA extracted at days, 17, 30, and 60 against the 0 day extracted (Fig. 5*B*; Supplementary Fig. S7). To exclude the possibility of a cell culture effect, the DNA of the noninduced cells from the same time points was also examined, showing no alterations (data not shown). SNP oligonucleotide

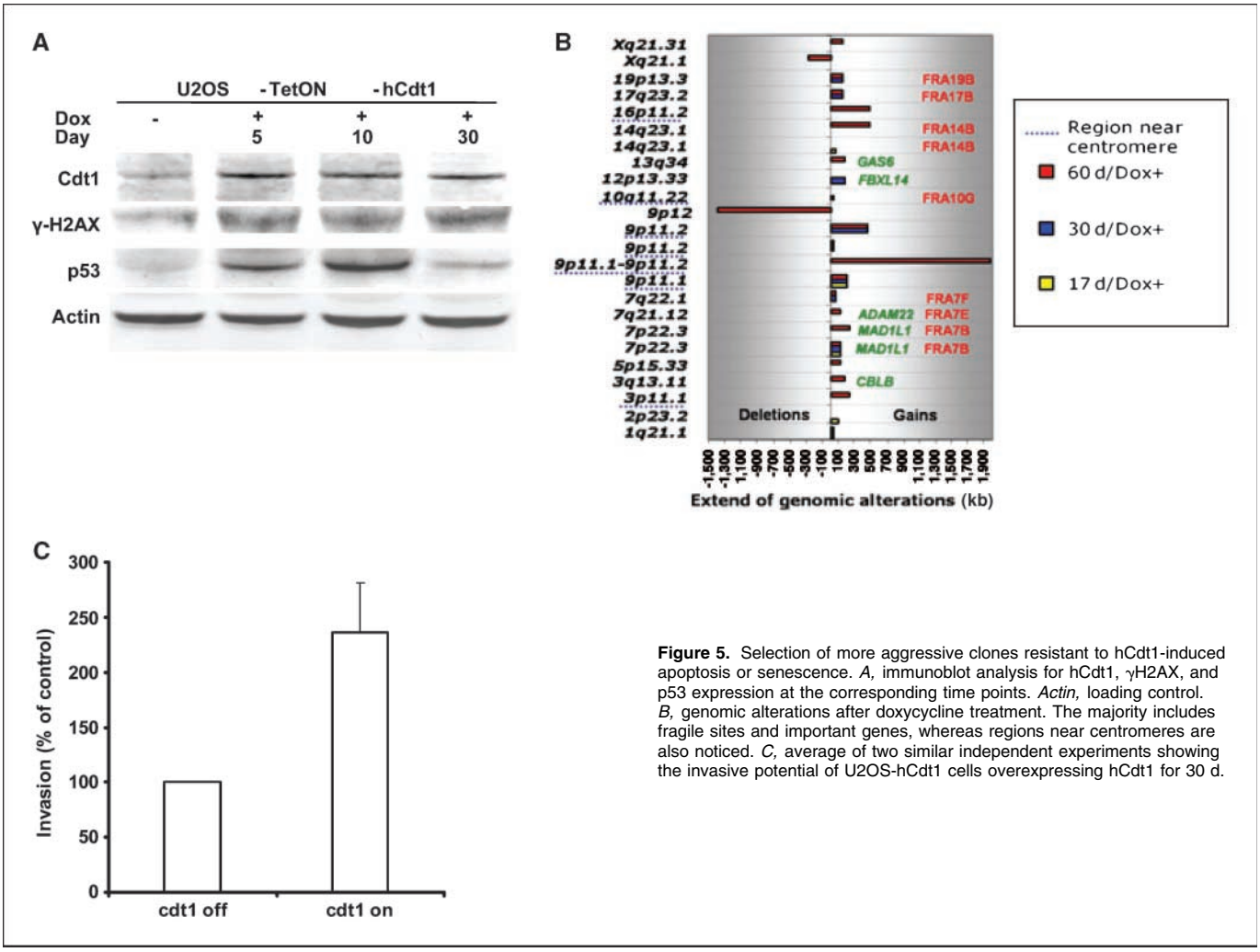

Figure 5. Selection of more aggressive clones resistant to hCdt1-induced apoptosis or senescence. *A,* immunoblot analysis for hCdt1, γH2AX, and p53 expression at the corresponding time points. *Actin,* loading control. *B,* genomic alterations after doxycycline treatment. The majority includes fragile sites and important genes, whereas regions near centromeres are also noticed. *C,* average of two similar independent experiments showing the invasive potential of U2OS-hCdt1 cells overexpressing hCdt1 for 30 d.

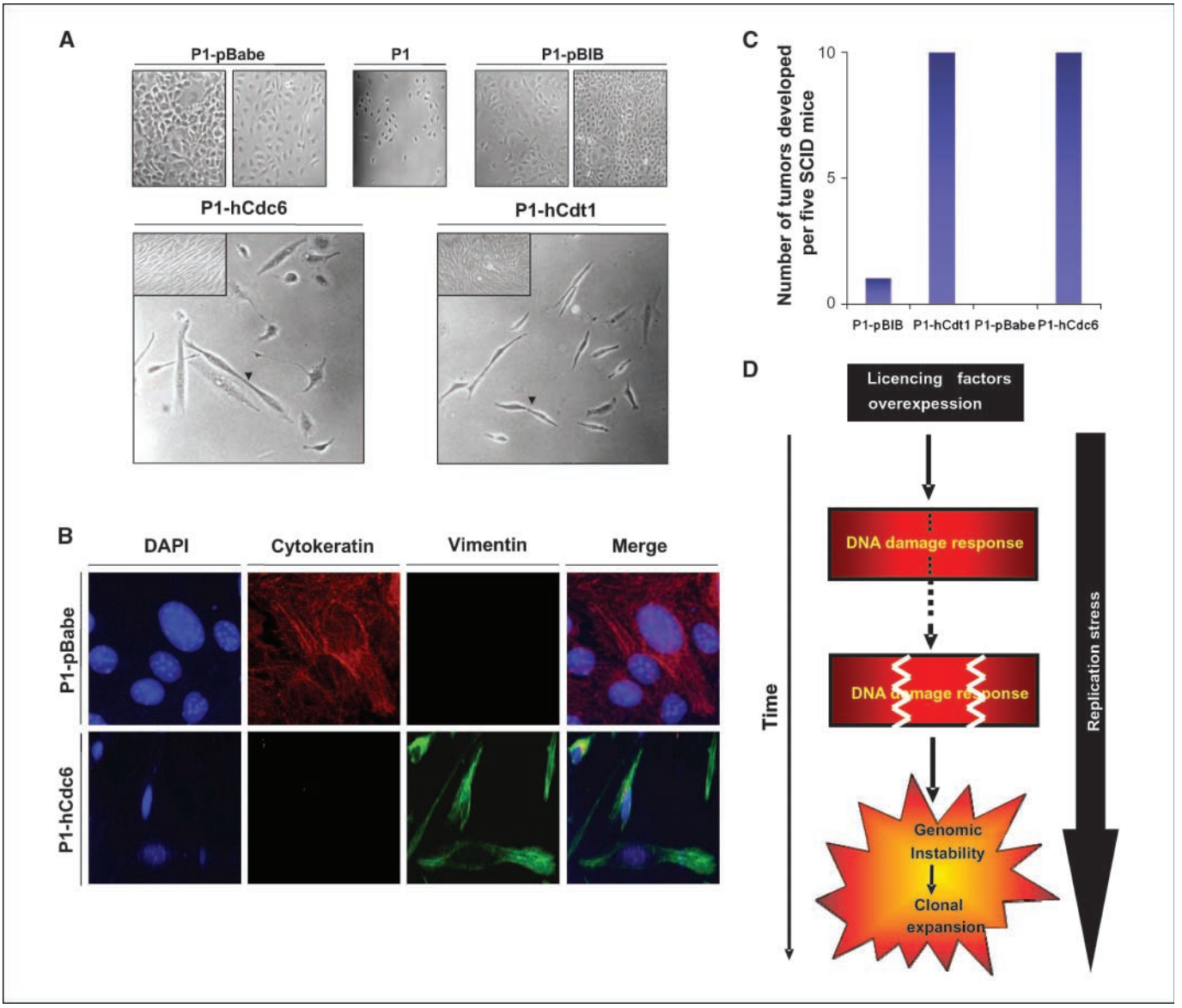

Figure 6. *A,* stable expression of hCdt1 and hCdc6 in papilloma P1 leads to cellular transformation. *Black arrowheads,* nucleoplasmic bridges. *B,* double immunofluorescence analysis for cytokeratin (anticytokeratin, rabbit polyclonal, A0575, DAKO) and vimentin [antivimentin, mouse monoclonal (clone V9), isotype: IgG1, κ, DAKO] in P1-hCdc6 and the corresponding mock cells. Similar results were found in P1-hCdt1 cells (data not shown). *C,* tumorigenicity assay of P1-pBabe-hCdt1 and P1-pBIB-hCdc6 cells and their corresponding mock cells in SCID mice. *D,* model showing that licensing factor deregulation, via replication stress, exerts pressure on the DDR machinery, which eventually collapses, leading to genomic instability and clonal expansion of cells.

microarray analysis showed gradual increase in genomic alterations, mainly gains, in an additive manner, ranging from 37 kb to 1.9 Mb (Fig. 5*B*; Supplementary Fig. S7). Fragile sites, areas of the genome prone to breaks and recombinations, were more frequently affected (38% of all affected sites; Fig. 5*B*; refs. 32, 44, 45), supporting the notion of genomic reformation/recombination proposed earlier. Among impaired chromosomal regions was *7p22.3*, which contains part of the *mitotic arrest deficient-like 1* (*MAD1L1*) gene (Fig. 5*B*). *MAD1L1* is essential for the mitotic spindle assembly checkpoint that monitors chromosomal segregation fidelity, guarding against the emergence of aneuploidy (46). Alteration at this specific chromosomal area could perturb the normal function of *MAD1L1*, affecting the mitotic checkpoint participating in the increased aneuploidy observed after day 15 (Fig. 5*B*). Another gene possibly affected is *GAS6* (*growth arrest–specific gene 6*; *13q34*; Fig. 5*B*). Overexpression of GAS6 and its receptor tyrosine kinase Axl has been associated with various carcinomas (47) and could contribute to the aggressiveness of the arisen clone.

To investigate whether the acquired genomic alterations resulted in a more aggressive behavior, we examined the invasive properties of the evolved hCdt1 clones. Invasion and metastasis are the hallmarks distinguishing malignancy from benign conditions. To this end, an invasion assay was done between the induced and noninduced at day 30. The former cells possessed a significantly more potent invasion potential compared with the latter ones, supporting the notion that genomic instability fuels premalignant and malignant cells with mutations that promote their selective advantage (ref. 48; Fig. 5*C*).

Stable hCdt1 and hCdc6 expression in papilloma-premalignant cells leads to cellular transformation. The hCdt1 and hCdc6 role in early stages of carcinogenesis was further addressed by examining their stable overexpression effects in the mouse papilloma P1 cells. P1 are papilloma lines isolated from 7,12-dimethylbenz(*a*)anthracene (DMBA)/12-*O*-tetradecanoylphorbol-13-acetate (TPA)–treated *spretus* × CBA F_1 mice (49). Generally, they are nontumorigenic when injected s.c. into nude mice, although occasionally at the injection sites either benign cysts or well-differentiated tumors are seen (49). *In vitro* P1 cells have a typical epithelial morphology being cuboidal in shape, with a cobblestone pattern of growth (Fig. 6*A*). At the molecular level, they posses a 2:1 mutant to wild-type H-*ras* alleles, due to a chromosome 7 trisomy (49). The nontumorigenic nature of these cells renders them as an appropriate premalignant epithelial cellular system to study the transformation potential of putative oncogenes.

The high *Cdt1* and *Cdc6* sequence homology between human and mouse, respectively, and the reported ability of the human *Cdt1* and *Cdc6* to function within the mouse environment (8), led us to human retroviral constructs infection of P1 cells. During the course of selection, the P1 cells started to acquire a spindle-fibroblastoid morphology that was evident in both subconfluent and confluent cell culture conditions while mock cells retained their epithelial morphology (Fig. 6*A*). Certain morphologic features observed in the activated U2OS-TetON-hCdt1 system, such as nucleoplasmic bridges and micronuclei (Fig. 6*A*), which are indicative of DNA misrepair, chromosome rearrangement, and generally genomic instability (40), were present in the P1-hCdt1 and P1-hCdc6 as well. After 2 weeks of selections, clones were picked up and propagated, and hCdt1 and hCdc6 expression was confirmed (data not shown). Interestingly, the clones, in both cases, had a uniform spindle appearance highly reminiscent of the spindle-fibroblastoid morphology of the cell lines A5 and CarB, which represent the most aggressive cellular type of the mouse skin model (49). In agreement, the immunofluorescent evaluation of cell intermediate filament status revealed a shift from a keratin-rich network in the parental P1 and mock cells to a vimentin-rich network in the P1-hCdt1 and P1-hCdc6 cells, indicative of an epithelial to mesenchymal transition of the clones, also seen in A5 and CarB cell lines (Fig. 6*B*; ref. 50).

To examine the P1-hCdt1 and P1-hCdc6 tumorigenicity, we injected them s.c. at two sites on the one side of the abdominal region of SCID mice, whereas, on the other side mock cells were injected as controls. Within a period of 2 to 3 weeks, all P1-hCdt1 and P1-hCdc6 injected sites gave rise to tumors (20 of 20, 100%) whereas the P1 mock cells gave tumors only in 1 of 20 sites (5%; Fig. 6*C*).

Altogether, our results support the oncogenic potential of overexpressed hCdt1 and hCdc6 from the earliest stages of carcinogenesis. This is achieved by rereplication and generation of DSBs. Initially, these events activate the antitumor barriers of senescence and apoptosis but eventually are bypassed by the continuous hCdt1 and hCdc6 stimulus, which induce genomic instability favoring clonal expansion of cells with more aggressive properties (Fig. 6*D*).

Acknowledgments

Received 7/25/2007; revised 9/11/2007; accepted 9/21/2007.

Grant support: Danish Cancer Society, Danish National Research Foundation, grant MSM-6198959216, and European Commission (integrated projects "Active p53" and "Mutant p53"; J. Bartkova and J. Bartek).

The costs of publication of this article were defrayed in part by the payment of page charges. This article must therefore be hereby marked *advertisement* in accordance with 18 U.S.C. Section 1734 solely to indicate this fact.

We thank Dr. Allan Balmain for kindly providing the P1 cells and Dr. George Kotzamanis for his valuable help with the pulse field gel electrophoresis.

References

1. Bartek J, Lukas J. DNA damage checkpoints: from initiation to recovery or adaptation. Curr Opin Cell Biol 2007;19:238–45.
2. Bartkova J, Rezaei N, Liontos M, et al. Oncogene-induced senescence is part of the tumorigenesis barrier imposed by DNA damage checkpoints. Nature 2006;444:633–7.
3. Gorgoulis VG, Vassiliou LV, Karakaidos P, et al. Activation of the DNA damage checkpoint and genomic instability in human precancerous lesions. Nature 2005;434:907–13.
4. Bartkova J, Horejsi Z, Koed K, et al. DNA damage response as a candidate anti-cancer barrier in early human tumorigenesis. Nature 2005;434:864–70.
5. Mailand N, Diffley JF. CDKs promote DNA replication origin licensing in human cells by protecting Cdc6 from APC/C-dependent proteolysis. Cell 2005;122:915–26.
6. Nishitani H, Lygerou Z. Control of DNA replication licensing in a cell cycle. Genes Cells 2002;7:523–34.
7. Vaziri C, Saxena S, Jeon Y, et al. A p53-dependent checkpoint pathway prevents rereplication. Mol Cell 2003;11:997–1008.
8. Tatsumi Y, Sugimoto N, Yugawa T, Narisawa-Saito M, Kiyono T, Fujita M. Deregulation of Cdt1 induces chromosomal damage without rereplication and leads to chromosomal instability. J Cell Sci 2006;19:3128–40.
9. Karakaidos P, Taraviras S, Vassiliou LV, et al. Overexpression of the replication licensing regulators hCdt1 and hCdc6 characterizes a subset of non-small-cell lung carcinomas: synergistic effect with mutant p53 on tumor growth and chromosomal instability—evidence of E2F-1 transcriptional control over hCdt1. Am J Pathol 2004;165:1351–65.
10. Gonzalez S, Klatt P, Delgado S, te al. Oncogenic activity of Cdc6 through repression of the INK4/ARF locus. Nature 2006;440:702–6.
11. Murphy N, Ring M, Heffron CC, et al. p16INK4A, CDC6, and MCM5: predictive biomarkers in cervical preinvasive neoplasia and cervical cancer. J Clin Pathol 2005;58:525–34.
12. Bonds L, Baker P, Gup C, Shroyer KR. Immunohistochemical localization of Cdc6 in squamous and glandular neoplasia of the uterine cervix. Arch Pathol Lab Med 2002;126:1163–8.
13. Xouri G, Lygerou Z, Nishitani H, Pachnis V, Nurse P, Taraviras S. Cdt1 and geminin are down-regulated upon cell cycle exit and are over-expressed in cancer-derived cell lines. Eur J Biochem 2004;271:3368–78.
14. Bravou V, Nishitani H, Song SY, Taraviras S, Varakis J. Expression of the licensing factors, Cdt1 and Geminin, in human colon cancer. Int J Oncol 2005;27:1511–8.
15. Gorgoulis V, Zoumpourlis V, Rassidakis G, et al. Molecular analysis of p53 gene in laryngeal premalignant and malignant lesions. p53 protein immunohistochemical expression is positively related to proliferating cell nuclear antigen labelling index. Virchows Arch 1995;426:339–44.
16. Jiang W, Wells NJ, Hunter T. Multistep regulation of DNA replication by Cdk phosphorylation of HsCdc6. Proc Natl Acad Sci U S A 1999;96:6193–8.
17. Nishitani H, Taraviras S, Lygerou Z, Nishimoto T. The human licensing factor for DNA replication Cdt1 accumulates in G1 and is destabilized after initiation of S-phase. J Biol Chem 2001;276:44905–11.
18. Koutsami MK, Tsantoulis PK, Kouloukoussa M, et al. Centrosome abnormalities are frequently observed in non-small-cell lung cancer and are associated with aneuploidy and cyclin E overexpression. J Pathol 2006;209:512–21.
19. Santoni-Rugiu E, Duro D, Farkas T, et al. E2F activity is essential for survival of Myc-overexpressing human cancer cells. Oncogene 2002;21:6498–509.
20. Gorgoulis VG, Zacharatos P, Mariatos G, et al. Deregulated expression of c-mos in non-small cell lung carcinomas: relationship with p53 status, genomic instability, and tumor kinetics. Cancer Res 2001;61:538–49.
21. Al-Romaih K, Bayani J, Vorobyova J, et al. Chromosomal instability in osteosarcoma and its association with centrosome abnormalities. Cancer Genet Cytogenet 2003;144:91–9.
22. Petersen BO, Lukas J, Sorensen CS, Bartek J, Helin K. Phosphorylation of mammalian CDC6 by cyclin A/CDK2 regulates its subcellular localization. EMBO J 1999;18:396–410.
23. Tsantoulis PK, Gorgoulis VG. Involvement of E2F transcription factor family in cancer. Eur J Cancer 2005;41:2403–14.
24. Fujita M. Cdt1 revisited: complex and tight regulation during the cell cycle and consequences of deregulation in mammalian cells. Cell Div 2006;17:22.
25. O'Keefe LV, Richards RI. Common chromosomal fragile sites and cancer: focus on FRA16D. Cancer Lett 2006;232:37–47.
26. Levy B, Hirschhorn K. Protocols and Applications

(Methods in Molecular Biology). In: Fan Y-S, editor. Molecular Cytogenetics. Humana Press; 2002. p. 121.
27. Sekido Y, Fong KM, Minna JD. Progress in understanding the molecular pathogenesis of human lung cancer. Biochim Biophys Acta 1998;1378:F21–59.
28. Mao L, Lee JS, Fan YH, et al. Frequent microsatellite alterations at chromosomes 9p21 and 3p14 in oral premalignant lesions and their value in cancer risk assessment. Nat Med 1996;2:682–5.
29. DiTullio RA, Jr., Mochan TA, Venere M, et al. 53BP1 functions in an ATM-dependent checkpoint pathway that is constitutively activated in human cancer. Nat Cell Biol 2002;4:998–1002.
30. Lew DJ, Kornbluth S. Regulatory roles of cyclin dependent kinase phosphorylation in cell cycle control. Curr Opin Cell Biol 1996;8:795–804.
31. Bakkenist CJ, Kastan MB. DNA damage activates ATM through intermolecular autophosphorylation and dimer dissociation. Nature 2003;421:499–506.
32. Di Micco R, Fumagalli M, Cicalese A, et al. Oncogene-induced senescence is a DNA damage response triggered by DNA hyper-replication. Nature 2006;444:638–42.
33. Ferbeyre G, de Stanchina E, Querido E, Baptiste N, Prives C, Lowe SW. PML is induced by oncogenic ras and promotes premature senescence. Genes Dev 2000; 14:2015–27.
34. Pearson M, Carbone R, Sebastiani C, et al. PML regulates p53 acetylation and premature senescence induced by oncogenic Ras. Nature 2000;406:207–10.
35. Dellaire G, Ching RW, Ahmed K, et al. Promyelocytic leukemia nuclear bodies behave as DNA damage sensors whose response to DNA double-strand breaks is regulated by NBS1 and the kinases ATM, Chk2, and ATR. J Cell Biol 2006;175:55–66.
36. Bøe SO, Haave M, Jul-Larsen A, Grudic A, Bjerkvig R, Lønning PE. Promyelocytic leukemia nuclear bodies are predetermined processing sites for damaged DNA. J Cell Sci 2006;119:3284–95.
37. Serrano M, Lin AW, McCurrach ME, Beach D, Lowe SW. Oncogenic ras provokes premature cell senescence associated with accumulation of p53 and p16INK4a. Cell 1997;88:593–602.
38. Chen Z, Trotman LC, Shaffer D, et al. Crucial role of p53-dependent cellular senescence in suppression of Pten-deficient tumorigenesis. Nature 2005;436:725–30.
39. Nigg EA. Centrosome aberrations: cause or consequence of cancer progression? Nat Rev Cancer 2002;2: 815–25.
40. Fenech M. Cytokinesis-block micronucleus assay evolves into a "cytome" assay of chromosomal instability, mitotic dysfunction and cell death. Mutat Res 2006;600: 58–66.
41. Abulaiti A, Fikaris AJ, Tsygankova OM, Meinkoth JL. Ras induces chromosome instability and abrogation of the DNA damage response. Cancer Res 2006;66: 10505–12.
42. Castedo M, Perfettini JL, Roumier T, Andreau K, Medema R, Kroemer G. Cell death by mitotic catastrophe: a molecular definition. Oncogene 2004; 23:2825–37.
43. Illidge TM, Cragg MS, Fringes B, Olive P, Erenpreisa JA. Polyploid giant cells provide a survival mechanism for p53 mutant cells after DNA damage. Cell Biol Int 2000;24:621–33.
44. Popescu NC. Genetic alterations in cancer as a result of breakage at fragile sites. Cancer Lett 2003;192: 1–17.
45. Casper AM, Nghiem P, Arlt MF, Glover TW. ATR regulates fragile site stability. Cell 2002;111:779–89.
46. Malmanche N, Maia A, Sunkel CE. The spindle assembly checkpoint: preventing chromosome mis-segregation during mitosis and meiosis. FEBS Lett 2006;580:2888–95.
47. Hafizi S, Dahlback B. Signalling and functional diversity within the Axl subfamily of receptor tyrosine kinases. Cytokine Growth Factor Rev 2006;17:295–304.
48. Hanahan D, Weinberg RA. The hallmarks of cancer. Cell 2000;100:57–70.
49. Zoumpourlis V, Solakidi S, Papathoma A, Papaevangeliou D. Alterations in signal transduction pathways implicated in tumour progression during multistage mouse skin carcinogenesis. Carcinogenesis 2003;24: 1159–65.
50. Lee JM, Dedhar S, Kalluri R, Thompson EW. The epithelial-mesenchymal transition: new insights in signaling, development, and disease. J Cell Biol 2006; 172:973–81.